Valagiannopoulos, Constantinos A.; Mirmoosa, Mohammad S.; Nefedov, Igor S.; Tretyakov, Sergei A.; Simovski, Constantin R.

Hyperbolic-metamaterial antennas for broadband enhancement of dipole emission to free space

Published in:
Journal of Applied Physics

DOI:
10.1063/1.4900528

Published: 01/01/2014

Document Version
Publisher's PDF, also known as Version of record

Please cite the original version:
Valagiannopoulos, C. A., Mirmoosa, M. S., Nefedov, I. S., Tretyakov, S. A., & Simovski, C. R. (2014). Hyperbolic-metamaterial antennas for broadband enhancement of dipole emission to free space. *Journal of Applied Physics*, *116*(16). https://doi.org/10.1063/1.4900528

Hyperbolic-metamaterial antennas for broadband enhancement of dipole emission to free space

C. A. Valagiannopoulos, M. S. Mirmoosa, I. S. Nefedov, S. A. Tretyakov, and C. R. Simovski

Citation: Journal of Applied Physics **116**, 163106 (2014); doi: 10.1063/1.4900528
View online: https://doi.org/10.1063/1.4900528
View Table of Contents: http://aip.scitation.org/toc/jap/116/16
Published by the American Institute of Physics

JOURNAL OF APPLIED PHYSICS **116**, 163106 (2014)

Hyperbolic-metamaterial antennas for broadband enhancement of dipole emission to free space

C. A. Valagiannopoulos,[1,2] M. S. Mirmoosa,[1] I. S. Nefedov,[1] S. A. Tretyakov,[1] and C. R. Simovski[1]

[1]*Department of Radio Science and Engineering, School of Electrical Engineering, Aalto University, P.O. Box 13000, FI-00076 Aalto, Finland*

[2]*Department of Electrical and Computer Engineering, University of Texas at Austin, 1616 Guadalupe St., Texas 78712, USA*

(Received 23 August 2014; accepted 15 October 2014; published online 29 October 2014)

Dipole emitters used in nano optics and nanophotonics (e.g., fluorescent molecules or quantum dots) are weak radiators and thus detecting the radiation of a single emitter gets possible only if it is significantly enhanced. For this enhancement, one often utilizes resonant nanoantennas (Purcell's effect); this method, however, requires the exact knowledge of source location and radiation frequency which constitute a significant drawback. One known possibility for broadband location-insensitive radiation enhancement is to use a layer of the so-called hyperbolic metamaterial. However, the enhanced radiated energy is mainly directed into the volume of the lossy medium, where it is lost to heating. In this work, we suggest specific shapes of macroscopic hyperbolic metamaterial samples to open radiation windows for enhanced radiation to free space. We show that hyperbolic media slabs with properly shaped macroscopic grooves convert the evanescent waves produced by a dipole into waves traveling in free space, which results in the enhancement of useful radiation by one to two orders of magnitude. That level of enhancement of radiation into free-space which is also wideband and of non-resonant nature has not been reported up to now. These results may open possibilities for realization of broadband and directive antennas, where the primary radiators are randomly positioned fluorescent molecules or quantum dots. [http://dx.doi.org/10.1063/1.4900528]

I. INTRODUCTION

A. Enhancement of radiation

Electrically (optically) small objects are very poor and inefficient radiators of electromagnetic waves. In the antenna terminology, radiation ability of an antenna is characterized by its radiation resistance, which behaves as $(l/\lambda)^2$ for small electric dipole radiators. Here, l is the radiator size and λ is the wavelength in the surrounding space. At radio and microwave frequencies, this problem is conventionally overcome with the use of antennas. Usual antennas are structures which have the dimensions comparable or larger than the wavelength, allowing huge radiation enhancement due to electrically large apertures and activated resonances. In the optical domain, similar results can be achieved with the use of nanoantennas, which are, basically, resonant objects brought close to a deeply subwavelength light source.

In the optical literature, this effect of radiation enhancement is called Purcell's effect, and the radiated power increase factor is called Purcell's factor. In most common schemes these resonators are plasmonic nanoantennas, e.g., bow-tie structures formed by two silver or gold triangular patches of submicron dimensions (see e.g., indicative works[1,2]). For the antenna to operate, the primary radiating nanoobject must be precisely positioned with respect to the antenna, for example, in the gap between the two arms of a bow-tie nanostructure, and the resonance frequency of the antenna should match the frequency of the radiating molecule or nanoparticle. In many practical situations small radiating or scattering particles may be located at some random points at a surface, moreover, in the presence of many (and possibly different) emitting molecules or particles the radiation frequency may vary in a wide range of frequencies. Obviously, within this scenario, nanoantennas cannot be used to provide an effective radiation channel and couple the particles with waves propagating in free space. In this paper we will propose means to enhance dipole radiation in these situations.

To quantify the increase of radiated power of a given small source due to a non-resonant environment, we will use the ratio of the radiated powers in the presence and absence of the radiation-enhancement structure. If the dipole moment of the source is fixed and does not depend on the environment, this ratio is equal to the ratio of the corresponding radiation resistances, and in the case of a resonant nanoantenna it is equivalent to the conventionally used Purcell's factor F_P.[3] We assume that the size of the antenna is finite, and our goal is to find means to enhance radiation into surrounding free space. To account for possible losses of power in the antenna itself, we take the ratio of powers propagating in free space, in the far zone of the antenna. This figure of merit we will call *Enhancement of Useful Radiation* or $\mathcal{EUR}$.

Probably the simplest possibility to enhance power radiated from a small emitter whose location cannot be fixed and when the radiation frequency is not exactly known is to position the emitter in a homogeneous lossless dielectric medium (refractive index n). It is well known that the radiation resistance of a dipole with the dipole moment **p** located in a usual dielectric with refractive index n is n times larger than that of the same dipole $\mathbf{p}$ in free space.[4] However, this radiated power increase refers to the power radiated into this surrounding medium. To allow radiation into free space, the dielectric sample must be of a finite size, and reflections at the interface with the surrounding free space will reduce $\mathcal{EUR}$. Using the normal-incidence reflection coefficient at the dielectric-vacuum interface, the total radiation increase factor can be estimated as $4n^2/(n+1)^2$, which cannot exceed the value of 4 for $n>0$. Theoretically, this difficulty can be lifted using shells of materials with equal relative permittivity and permeability, because the interface with vacuum can be matched, eliminating normal-incidence reflections. However, this cannot be directly realized due to the absence of non-resonant magnetic materials at high frequencies. Note that in the regime of $n=-1$, the dielectric cover acts as a resonant antenna, which is not suitable for our present goals.

B. Use of hyperbolic media

Practically realizable possibilities for strong broadband enhancement of radiation using non-resonant materials appear if one uses so called hyperbolic media.[5] Hyperbolic metamaterial (HMM) is an optically uniaxial material, whose electromagnetic properties can be described in the condensed form by effective relative permittivity tensor (with optical applications in mind, we consider only non-magnetic media),

$$\bar{\bar{\varepsilon}} = \begin{pmatrix} \varepsilon_{||} & 0 & 0 \\ 0 & \varepsilon_{\perp} & 0 \\ 0 & 0 & \varepsilon_{\perp} \end{pmatrix}, \tag{1}$$

such that the diagonal components $\varepsilon_{||}$ and $\varepsilon_{\perp}$ have different signs. More specifically, in HMM this property concerns the real parts of these complex values: $\Re[\varepsilon_{||}]\Re[\varepsilon_{\perp}]<0$ (whereas the imaginary parts are assumed to be sufficiently small, i.e., $|\Im[\varepsilon_{\perp,||}]| \ll |\Re[\varepsilon_{\perp,||}]|$). In contrast to conventional anisotropic dielectrics where the permittivity tensor is positive-definite and to plasmas where it is negative-definite, in hyperbolic media the permittivity tensor does not belong to any of these two classes; therefore, HMMs are also called indefinite media.[6] This difference in signs makes the HMM operate as a conventional magneto-dielectric for waves, propagating along one direction, and as a metal for waves propagating along another direction, perpendicular to the first one. The word hyperbolic in the name of these composite media comes from the shape of the isofrequency contours that describe the solution of the dispersion equation in a uniaxial medium for the case $\varepsilon_{||}<0$ and $\varepsilon_{\perp}>0$,

$$\frac{q_x^2}{\varepsilon_{\perp}} - \frac{q_t^2}{|\varepsilon_{||}|} = k_0^2, \tag{2}$$

which permits infinitely large wavenumbers q for a lossless material. Similar formulas are obtained for the case when $\varepsilon_{||}>0$ and $\varepsilon_{\perp}<0$. Here $\mathbf{q}=(q_x,q_y,q_z)$ is the wave vector in the HMM, $q_t=\sqrt{q_y^2+q_z^2}$ is its transverse component and $k_0=\omega/c=2\pi/\lambda_0$ is the wavenumber in free space. The time dependence is selected in the form $\exp(+j\omega t)$.

A remarkable property of a dipole source embedded in such a medium is strong enhancement of radiation and a very specific radiation pattern called radiation cones. The enhancement of radiation is related with the elimination of reactive electromagnetic power usually stored in the vicinity of a dipole source in the form of evanescent waves whose magnetic field vector is orthogonal to the medium axis (TM-waves). No restriction to the wave number q of propagating waves means that all TM-polarized spatial harmonics produced by a dipole are propagating and the electromagnetic energy of TM-waves completely irradiates, that is, the radiation resistance is theoretically infinite. The effect of radiation cones means that the radiated field is concentrated at a bi-conical surface whose apex is the source point. In other words, the radiated wave inside the hyperbolic medium does not diverge and its field is not inversely proportional to the propagation path unlike usual dielectric media. In the case of realistic (lossy) HMM, the radiated field retains a high magnitude across this bi-conical surface, even at optically large distances from the source and decays exponentially versus the distance from the radiation cones.

Radiation cones were first predicted[7] for a cold strongly magnetized plasma operating at radio frequencies. Such plasma also possesses an indefinite permittivity tensor $\Re[\varepsilon_{||}]\Re[\varepsilon_{\perp}]<0$ and, therefore, hyperbolic dispersion.[8] Giant enhancement of radiation of a dipole antenna in a cold magnetized plasma has been also claimed;[9] however, calculations in that work were incorrect.[10] Correct calculations of the radiated power for a point dipole in a lossless cold magnetized plasma[11] have shown the infinite value for its radiation resistance. The radiated power remains finite if we realistically assume that the source has a finite size, instead of considering a point dipole.[12] Radiation enhancement for a short dipole antenna located in cold magnetized plasma operating at radio frequencies was measured in paper.[10]

In several works,[13–16] Purcell's factor of a uniform unbounded HMM was studied. In these papers, the authors took into account the geometry and sizes of dipole emitters, optical losses in realistic HMM, and its internal granularity. Purcell's factor of a realistic HMM has the order of magnitude between $(\lambda/a)^2$ and $(\lambda/a)^3$, where λ is the effective wavelength in the dielectric constituent of HMM and a is the period of the lattice of metallic constituents.[5] Practically, the enhancement can be as high as 10^2-10^4. Unfortunately, so high values of Purcell's factor do not imply strong radiation through the interface HMM-free space due to the total internal reflection of waves whose transverse wave vector components exceed k_0, and no significant enhancement of useful radiation ($\mathcal{EUR}$) has been achieved. Most part of radiation is directed into the metamaterial substrate and is spent to its heating like it holds for embedded sources.[17] Enhancement of useful radiation to free space happens only due to the thickness (Fabry-Perot) resonance of the HMM sample. However, this is a narrowband resonant effect, which refers to the classical Purcell's effect due to coupling of a dipole emitter to a resonator.[18] A common feature of any resonant scheme is a narrow frequency band of the enhanced emission and the necessity to engineer the resonance at the emission frequency. The last requirement makes the fabrication of the structure rather challenging, and this approach is not possible if the radiation frequency is not exactly known.

To achieve strong $\mathcal{EUR}$ to free space, one needs to control transformation of spatial spectrum which accompanies refraction at the material-air interface. To let the waves with large wavenumbers $|q| > k_0$ escape from the sample to free space, we need to somehow transform them into waves with wavenumbers $|q| < k_0$. An evident way to do it is to locate a well-known Kretschmann prism with refractive index $n > 1$ on the surface of a HMM sample. The waves $|q| < k_0 n$ will be propagating inside the prism and some of them can be diverted to its output surface at the angles below the angle of total internal reflection. This method was used[19] to convert waves propagating in a dielectric into free-space radiation. However, for dielectrics with negligibly small losses in the optical range we cannot have $n > 2.4 - 2.5$, and $\mathcal{EUR}$ due to such a prism cannot practically exceed 2. It has been also suggested[20] to texture the surface of the HMM sample transforming it into as a facet with period $a \ll \lambda$. This periodically textured surface efficiently scatters the internal waves with tangential wave numbers $q_y \approx \pi m/a$ (here m is an integer number, and axis y is directed along the surface). These waves are irradiated with wavenumbers $k_y = q_y - \pi m/a$ which for some m are smaller than k_0. However, in the absence of the resonance of the grooves[18] such patterning is not very efficient due to a narrow spatial spectrum of metamaterial eigenmodes converted into useful radiation.

In this paper, we suggest a way to achieve a broadband, non-resonant enhancement of useful dipole radiation using a properly shaped macroscopic metamaterial sample. We may modify both front and rear (with respect to the source) surfaces or only one of them. The governing idea is based on the fact that the tilt of an optical axis (OA) of HMM with respect to the interface allows conversion of waves with $|q| > k_0$ into waves with $|q| < k_0$ and vice-versa when the wave transmits through the interface. This conversion may happen for a very broad (theoretically infinite) spatial spectrum, which becomes possible due to concentration of radiated power in radiating cones, discussed above. The exploited effect has nothing to do with any resonance phenomena, and we test the non-resonant nature of the radiation enhancement for every single of the proposed configurations. It becomes feasible by avoiding to optimize the structure with respect to the variables that are responsible for possible resonances (such as frequency) and, once we have concluded to the optimal design, by representing $\mathcal{EUR}$ as a function of these "resonance variables" to ensure that the selected combination of variables does not give a global optimum. This novel mechanism of $\mathcal{EUR}$, in accordance to our calculations, can compete with the aforementioned result[18] in terms of the enhancement coefficient values. However, the use of the proposed here non-resonant mechanism makes the phenomenon broadband and does not require fitting the constitutive parameters of HMM to the frequency of the source. The idea of using a wedge-shaped sample with a tilted axis to convert evanescent waves into waves propagating in free space was elaborated in our works.[21,22] Earlier, obliquely cut samples of hyperbolic media were used in Ref. 23 for a different purpose. Interface coupling of HMM modes with very large wavenumbers to free-space modes when the optical axis is tilted with respect to the interface plane has been previously described also in papers[25,26] in relation to the studies of absorption of waves incident from free space. Furthermore, a recent review paper[24] analyzes the role of anisotropic plasmonic metamaterials in constructing hyperlenses.

II. SUGGESTED METAMATERIAL STRUCTURES

A dipole located on the surface of a HMM sample generates evanescent waves with wave numbers $|q| > k_0$. These waves transmitted into HMM are converted into propagating eigenmodes of HMM. If the rear interface of the sample is parallel to the front one, the eigenwaves, passing through the second interface, transform again into evanescent waves of free space. If the two surfaces are not parallel, the fields even after their transmission through the rear interface may remain propagating. This simple speculation results in the idea of an HMM wedge. The evanescent waves produced at the front side of the wedge convert into propagating waves irradiated from its rear side, as it was first noticed in our works.[21,22] The governing idea is illustrated by arbitrary (non-optimized) numerical simulation results shown in Fig. 1. If a sub-wavelength source (whose radiation into free space is illustrated in Fig. 1(a)) is close to a HMM slab, the power which the source radiates into the slab is strongly enhanced, and a typical radiation cone is formed (Fig. 1(b)). However, the radiated fields stay inside the slab, as the waves there have large wavenumbers, which are not supported by free space. A typical standing-wave pattern inside the slab is created due to reflections at the slab boundary. The picture on the right shows that properly shaping the bottom interface (here we make a wedge-shape cut, Fig. 1(c)), we open a possibility for high-wavenumber waves traveling inside the slab to pass through the interface. We observe strong radiation through the wedge surface and formation of a typical focused antenna pattern.

The first structure we suggest here is a 2D biprism filled with an HMM as shown in Fig. 2. Here, the negative optical axis is stretched horizontally ($\Re[\varepsilon_{||}] < 0$). Let a number of poorly radiating point sources (blue dots) creating a broad spatial spectrum of evanescent waves be located on the concave part of the sample surface. The evanescent waves with the transverse wave numbers $k_y = K > k_0$ and $k_y = -K < -k_0$ (red arrows in the left side dispersion graph) that penetrate into the medium are transformed into propagating waves with the wave vectors $\mathbf{q}_1$ and $\mathbf{q}_2$ (green arrows in the left side dispersion graph), respectively. For the wave vector $\mathbf{q}_1$, the component parallel to the plane B_1B_2 is preserved, while the component of the wave vector $\mathbf{q}_2$ parallel to B_2B_3 is preserved (left side projection). At the rear surface, the waves $\mathbf{q}_1$ and $\mathbf{q}_2$ are transformed into propagating waves with the wave vectors $\mathbf{k}_1$ and $\mathbf{k}_2$. The dashed lines correspond to waves that are passing from a boundary (phase matching projections) and the vectors normal to the dispersion curves $\mathbf{u}_1, \mathbf{u}_2$ denote the group velocities. In this way, the energy which is normally stored in the evanescent waves

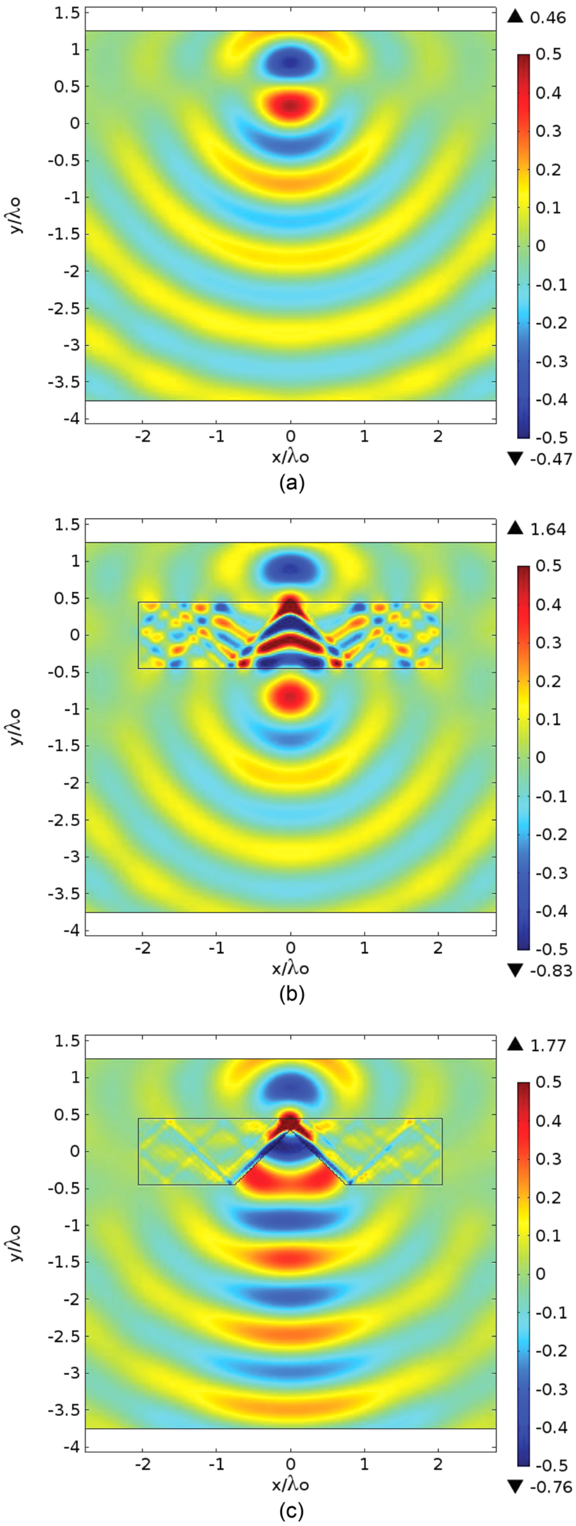

FIG. 1. A numerical illustration of the effect of shaping a HMM sample. (a) A cylindrical wave radiated by a dipole line (the radiating line is normal to the picture plane, and the dipole moment is in the horizontal plane). (b) Fields of the same source in the presence of a HMM slab. (c) The same, but the slab has a wedge-shaped cut, with the angle equal to the radiating cone angle. Plot parameters: $\varepsilon_\perp = \varepsilon_x = (4 - 0.08j)\varepsilon_0$, $\varepsilon_{||} = \varepsilon_y = (-4 - 0.08j)\varepsilon_0$.

$(K, j\sqrt{K^2 - k_0^2})$ and $(-K, j\sqrt{K^2 - k_0^2})$, will be radiated from the rear surface of the sample into free space.

The width of the spatial spectrum of evanescent waves converted into propagating ones using this approach depends

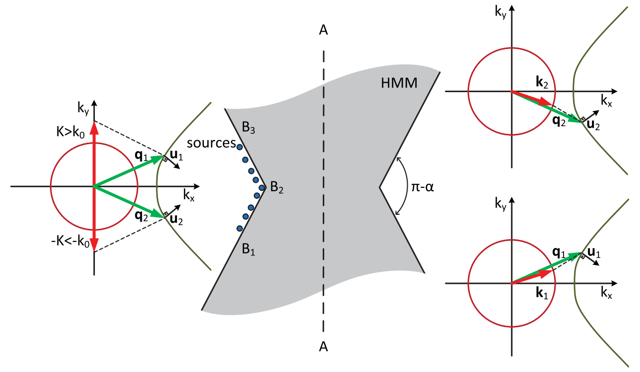

FIG. 2. The geometry of an HMM biprism with interfacial sources in the concave part. The negative axis of HMM is horizontal (x). Circles $k_x^2 + k_y^2 = k_0^2$ show the isofrequency contour of free space, hyperbolas correspond to the isofrequency contour of the HMM which determines the eigenmode wave vectors (e.g., $\mathbf{q}_1$ and $\mathbf{q}_2$). A theoretically infinite spatial spectrum of evanescent waves is partially transformed into waves irradiated from the rear surface (e.g., wave vectors $\mathbf{k}_1$ and $\mathbf{k}_2$). The corresponding pictures for the vertical direction of the negative axis of HMM show the same effect.

on the negative value $\varepsilon_\perp/\varepsilon_{||}$ (in the lossless case) and on the 2D biprism angle α. It is easy to show that under the condition $\varepsilon_{||}\cos^2\alpha + \varepsilon_\perp \sin^2\alpha = 0$ (the exact zero is possible if we neglect the losses in HMM) the whole spatial spectrum $0 < |K| < +\infty$ is effectively transformed to propagating waves at the rear interface since the tangential components are again matched (the right-side projection). More exactly, this important condition can be formulated as

$$\Re[\varepsilon_{||}]\cos^2\alpha + \Re[\varepsilon_\perp]\sin^2\alpha = 0. \tag{3}$$

Of course, even if this condition is satisfied, the conversion of every evanescent spatial harmonic into a propagating wave is only partial since at both interfaces waves experience partial reflections. Therefore, the optimal biprism angle α for given $\varepsilon_\perp$ and $\varepsilon_{||}$ may depend on other factors e.g., on the location of the source. Further, we consider the sources located near the front corner of the biprism at a small distance L from this corner. Note that the internal reflection of the waves propagating inside the HMM will result in the transformation of evanescent waves emitted by the source into propagating waves for the reflected field too. A thorough description of this conversion in the case of the wedge is given in earlier publications.[21,22]

In the 2D structure shown in Fig. 2, we neglect the components of the wave vectors that may be orthogonal to the plane xy. In fact, this figure refers to the case when the source is a line of dipoles (it may be e.g., a quantum wire). If the source is a point dipole, it produces also evanescent waves with $k_z = K > k_0$ and $k_z = -K < -k_0$ which can be converted into propagating ones. Then we come to a 3D analogue of Fig. 2—to the structure with two conical or pyramidal grooves. These 3D structures are expected to offer higher enhancements than the 2D biprism due to the presence of waves with nonzero k_z.

The same functionality as that illustrated by Fig. 2 is achievable in reflected fields if one puts a mirror at the plane A-A. Also, similar consideration as in Fig. 2 can be done for the case when the negative optical axis is vertical (along A-A). It is easy to see that the conversion of spatial spectrum occurs in this case under the same conditions. Furthermore, we understand that the role of the groove apex may be destructive because it may lead to the creation of a hot spot inside the metamaterial. Especially, this refers to the front groove since the source may be located near its apex. Since HMM has finite losses, the presence of a hot spot may cause high optical losses. Consequently, we may need to smooth the apex of the pyramidal or conical groove.

With this in mind, we come to a topology of a hemispherical notch (or semicircular cut in the 2D case). As to the opposite side of the sample, the conical or pyramidal groove (triangular cut in the 2D case) can be probably kept there. Due to the divergence of radiation propagating in the HMM, possible harmful influence of the apex on the rear side is less significant. This design solution is shown in Fig. 3. Alternatively, one can make a semicircular cut (spherical groove in the 3D case) also on the opposite side, as depicted in Fig. 4(a). Finally, if one is interested to obtain $\mathcal{EUR}$ in the reflected field, one comes to the structure shown in Fig. 4(b).

For all these structures, the $\mathcal{EUR}$ is *a priori* possible for both directions of the negative optical axis—vertical or horizontal. In the absence of a complete analytical model, it is difficult to predict which orientation of the dipole source is preferred in these cases. At the first glance, it seems that the dipole has to be oriented along the negative axis. Really, in the near electric field of an electric dipole the component parallel to its dipole moment is dominant. Therefore, such a dipole will be more strongly coupled to the metamaterial. If the dipole is orthogonal to the negative axis, its near electric field is mainly orthogonal to the negative axis, i.e., is mainly formed by the evanescent waves of TE-polarization. These waves are not transformed into propagating eigenmodes of the metamaterial—TE-polarization corresponds to ordinary waves in HMM. Therefore, the dipole directed along the negative axis seems to operate better than the dipole orthogonal to it. However, this speculation is very approximate and needs to be checked. In practice, a small radiator can be arbitrarily oriented and it creates evanescent waves with both TE- and TM-polarizations. Therefore, we assume an arbitrary dipole tilt angle θ with respect to the negative axis of HMM and check its impact on the structure performance.

The minimal distance between the front and rear surfaces is another parameter to be considered and optimized. Though we intentionally refuse to profit from the resonance of the whole HMM sample and of the grooves and consider their dimensions as macroscopic, the minimal thickness d of the sample (the distance between the grooves) cannot be optically very large. Otherwise, optical losses inherent to HMM will suppress the useful radiation. Evidently, the optimum of d has nothing to do with the thickness resonance. This optimum corresponds to a compromise between the amount of converted eigenmodes and their decay in the metamaterial bulk.

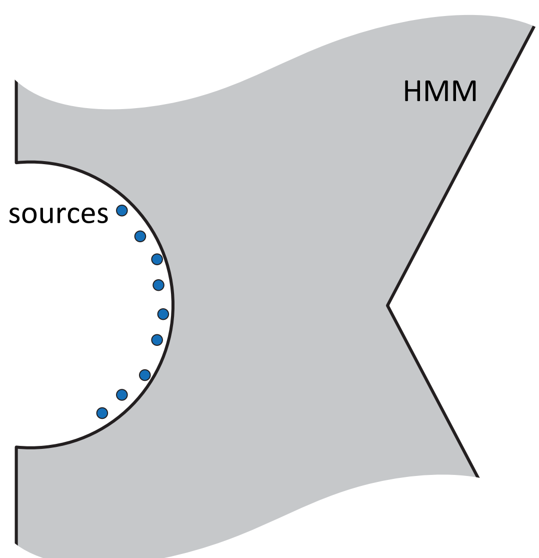

FIG. 3. Sketch of an alternative design: a triangular cut (pyramidal or conical groove in the 3D case) on the front side of the sample is replaced by a circular cut (a spherical groove in the 3D case).

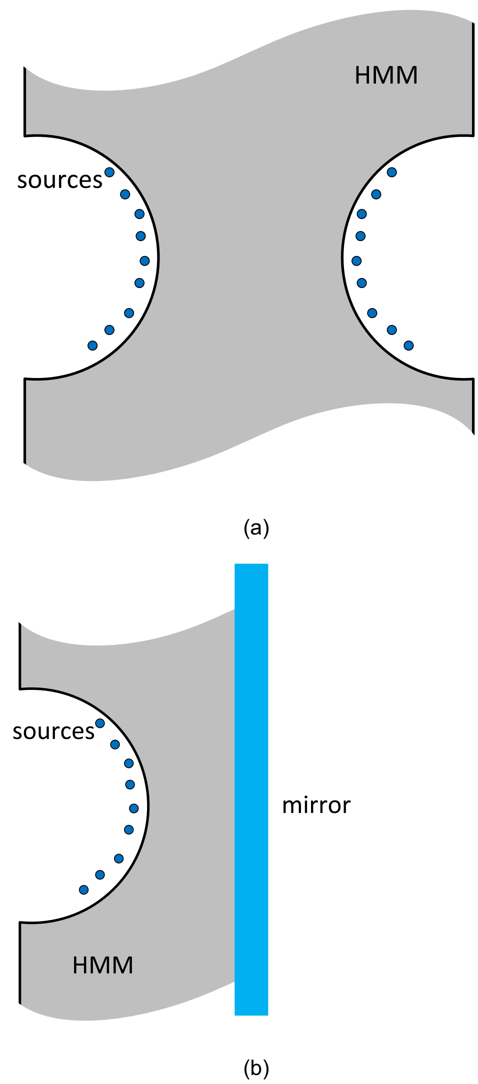

FIG. 4. Sketches of two design solutions. (a) A double concave lens of HMM and (b) a mirror-backed lens of HMM. Negative axis can be either parallel or orthogonal to the whole structure.

III. FULL-WAVE SIMULATIONS AND OPTIMIZATION

A. 2D geometries

Here, we numerically investigate three design solutions which correspond to Figs. 2, 3, and 4(a). The dimensions of the studied structures are given in Fig. 5. The structure depicted in Fig. 5(a) corresponding to our first suggestion is referred as the triangle-triangle design. The structure depicted in Fig. 5(b), corresponding to our second suggestion (the front cut is circular) is referred as the circle-triangle design. Finally, the structure depicted in Fig. 5(c) is referred as the circle-circle design. For all these structures, we study the enhancement of useful radiation $\mathcal{EUR}$ in transmitted fields (infinite semi-circle with $x > 0$). With this purpose, we optimize the following parameters of 2D structures depicted in Fig. 5: the minimal thickness d, the effective permittivities of HMM $\varepsilon_\perp, \varepsilon_\|$, and the optimal tilt angle θ for the dipole moment vector. We have inspected both possible orientations of the HMM negative axis in Fig. 5: along the x and y directions. We show only the results for the negative axis along the x axis ($\Re[\varepsilon_\|] < 0$). The alternative choice of the negative axis does not bring qualitatively new results.

The source is an electric dipole line,[11] i.e., an infinite line stretched along the z-axis with a uniformly distributed electric dipole moment, orthogonal to the line axis. The orientation of the dipole in the transverse plane is defined by the angle θ between the dipole direction and the horizontal axis, see Fig. 5. In the xy plane, the line source is initially located at the point $x = -d/2 - \delta$, $y = 0$ at a very small distance $\delta < d$ from the surface of HMM. The utilized software (COMSOL Multiphysics[27]) does not allow the dipole line to be located exactly at the sample surface, but δ can be arbitrarily small. In our simulations, the selection of δ was dictated by meshing limitations. It should be stressed that the line can move tangentially to the HMM surface, and we define its position by the distance L from the center, see Fig. 5.

Performing numerical simulations for macroscopic values of the dimensions G and g (Fig. 5), e.g., $G/\lambda_0, g/\lambda_0 \sim 10^3 - 10^4$ is impossible within realistic computation time; moreover, the convergence of simulations will be not achievable for so large sizes. Therefore, we have studied the trend of $\mathcal{EUR}$ when we increase these sizes, locating and excluding the resonances of our structures. Taking the values of sizes G and g which are reasonable compared to λ_0 but correspond to the macroscopic trend $G/\lambda_0, g/\lambda_0 \to +\infty$, we predict $\mathcal{EUR}$ for the macroscopic case. In this scenario, the only dimension to be optimized is the thickness d. After this optimization, we check the stability of the obtained $\mathcal{EUR}$ to deviations from the optimized parameters found earlier, such as the frequency ω and the source location, measured by the distance L.

According to our introductory description, the value of $\mathcal{EUR}$ for two-dimensional structures is computed by

$$\mathcal{EUR} = \lim_{R\to+\infty} \frac{\displaystyle\int_{-\pi/2}^{\pi/2} |\mathbf{E}(R,\phi)|^2 d\phi}{\displaystyle\int_{-\pi/2}^{\pi/2} |\tilde{\mathbf{E}}(R,\phi)|^2 d\phi}. \quad (4)$$

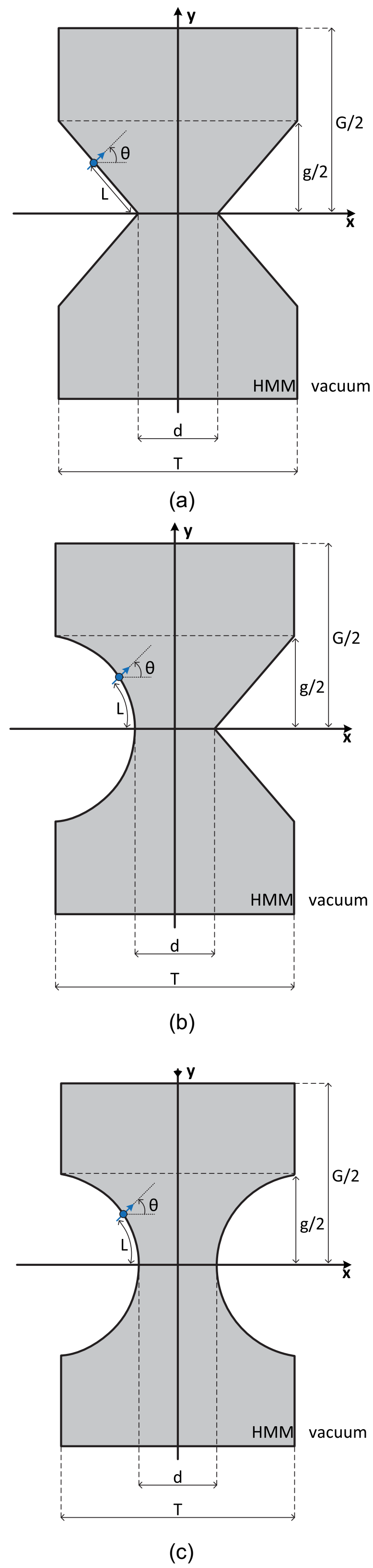

FIG. 5. The 2D configurations under numerical investigation. (a) A sample of hyperbolic metamaterial (HMM) with overall dimensions $T \times G$ has two symmetric triangular cuts of extent g (defining an angular extent of the prism α), so that the corners are separated by distance d. (b) The similar structure with the circular cut on the front side. (c) The similar structure with two circular cuts instead of triangles. All systems are excited by an electric dipole line at azimuthal distance L from the left groove's bottom, θ is the tilt of the dipole moment to the x-axis.

Here, $\mathbf{E}(\rho,\phi)$ is the electric field in presence of the structure numerically calculated and integrated over the right-hand side semi-circle of radius R (the source is on the left side of the sample). Here, we focus on the enhancement in transmission through the sample, but alternative performance indicators of the radiation enhancement can be given by taking into account the far-field radiation into the entire space. The notation $\tilde{\mathbf{E}}(\rho,\phi)$ is used for the electric field in the absence of the HMM antenna structure (in free space). The magnetic field of the dipole line in free space possesses solely an out-of-plane z component,

$$\tilde{H}_z(\rho,\phi) = H_1^{(2)}(k_0\rho)\sin(\phi-\theta), \tag{5}$$

where $\rho=\sqrt{(x-x_0)^2+(y-y_0)^2}$ ($\rho=0$ corresponds to the dipole line origin $(x_0,\ y_0)$), $\phi=\arctan(x-x_0,y-y_0)$ and symbol $H_1^{(2)}$ is used for the Hankel function. The electric field $\tilde{\mathbf{E}}(\rho,\phi)$ is analytically calculated from (5) via Maxwell's equations.

In our examples, the frequency for which the optimization has been done is equal to $\omega_0=600\pi$ Trad/s that corresponds to $\lambda_0=1\,\mu$m. The initial sizes for optimization are chosen as follows: $T=3\lambda_0, g=4\lambda_0, g=2\lambda_0$, $\Re[\varepsilon_\perp]=3.1\varepsilon_0$, $\Re[\varepsilon_\parallel]=-2.9\varepsilon_0$. Furthermore, the starting point for the orientation of the exciting dipole is: $\theta=45^\circ$ and for its position: $L=0$. In this section, we fix the losses of the parallel components at $\Im[\varepsilon_\parallel]=-0.2\varepsilon_0$ (that is typical for known HMM operating in the near infrared) and neglect losses for $\varepsilon_\perp$ (a reasonable approximation).

In Fig. 6(a), we show the quantity ($\mathcal{EUR}$) as a function of the distance d and we observe that in all cases the optimal result is achieved for $d=0.1\lambda_0$. For this choice, we represent the enhancement factor $\mathcal{EUR}$ with respect to the perpendicular permittivity $\varepsilon_\perp/\varepsilon_0$ (Fig. 6(b)), where different behavior of the three designs is spotted. The optimal performance points are selected and kept constant throughout the rest of the sweeping study. In Fig. 6(c), the varying parameter is the parallel permittivity $\varepsilon_\parallel/\varepsilon_0$ and the graph shapes are similar to the corresponding ones of Fig. 6(c). For two designs (triangle-triangle and circle-circle ones), the optimal ratio $|\Re[\varepsilon_\parallel]|/\Re[\varepsilon_\perp]$ is linked to the optimal prism angle α, since it is achieved for $|\Re[\varepsilon_\parallel]|\approx\Re[\varepsilon_\perp]$ whereas $\alpha\approx135^\circ$. So, the geometric-optical condition (3) offers nearly maximal $\mathcal{EUR}$ for these two designs. As to the circle-triangle design, the optimum was achieved for $\Re[\varepsilon_\perp]\approx5\varepsilon_0$ and $\Re[\varepsilon_\parallel]\approx-\varepsilon_0$. Equation (3) does not hold in this case; in particular, our initial parameters do not correspond to the macroscopic trend and thus our estimations based on the geometric optics are not applicable in this design. When it comes to Fig. 6(d), we find the best tilt angles for each of the three configurations. As was expected, it fits the simplistic estimation $\theta=0^\circ$ only for the circle-triangle and circle-circle geometries. This result confirms the adequacy of our speculations based on the geometric optics for the structure without an apex. Though the size of the cut in this case is only twice as large as λ_0, the dramatic shortening of the wave in the HMM makes geometric optics applicable. For the triangle-triangle structure with the source at $L=0$, the

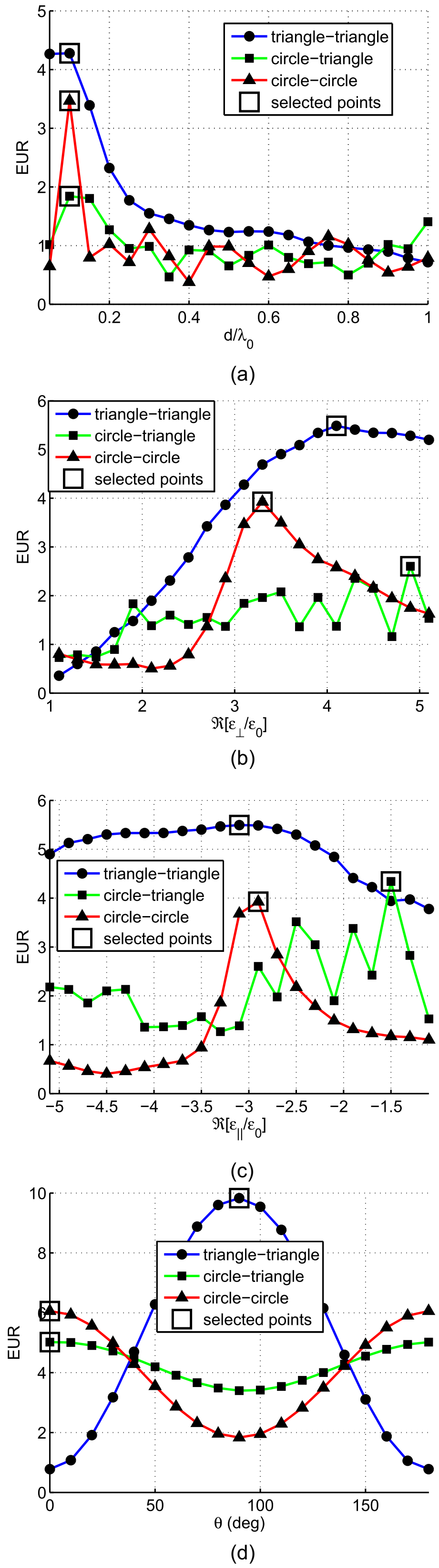

FIG. 6. The optimization graphs for the three 2D designs. (a) $\mathcal{EUR}$ as a function of the normalized distance between the notches d/λ_0, (b) $\mathcal{EUR}$ as a function of the perpendicular permittivity component of HMM $\Re[\varepsilon_\perp/\varepsilon_0]$, (c) $\mathcal{EUR}$ as a function of the parallel permittivity component of HMM $\Re[\varepsilon_\parallel/\varepsilon_0]$ and (d) $\mathcal{EUR}$ as a function of the tilt angle θ of the source. Triangle-triangle design (Fig. 5(a)) blue curves with circular dots, circle-triangle design (Fig. 5(b)) green curves with square dots, circle-circle design (Fig. 5(c)) red curves with triangular dots.

result is the opposite (the optimal $\theta = 90°$) due to the impact of the apex.

At the next stage, our goal is to confirm that the initial parameters found above correspond to the macroscopic trend $G/\lambda_0, g/\lambda_0$. To do that, we have calculated $\mathcal{EUR}$ for increasing dimensions G and g, keeping all the other parameters constant. For the triangle-triangle and circle-circle designs the conclusion is that already $G = 3\lambda_0$ corresponds to the macroscopic limit, as we do not observe significant changes increasing G/λ_0 up to 6. However, for the circle-triangle design where the initial parameters send us out of the macroscopic trend, the dependence on G keeps oscillating. As to the dependence on g/λ_0, the value of $\mathcal{EUR}$ for the circle-triangle and circle-circle designs weakly depends on this parameter in the range $3 < g/\lambda_0 < 6$. For the triangle-triangle design, $\mathcal{EUR}$ monotonically decreases with increasing g/λ_0. This is because for the smallest value of g/λ_0, the source is nearly at the apex of the double pyramid, which corresponds to the fronts of the two cones excited in the HMM sample. Further studies are made assuming $G = 4\lambda_0$ and $g = 2\lambda_0$.

The stability of $\mathcal{EUR}$ with respect to the frequency deviation ω/ω_0 and the deviation L/λ_0 of the source location is illustrated by Fig. 7. The first plot (Fig. 7(a)) shows that the enhancement which we have achieved is not an outcome of a resonance, since the selected points do not coincide with the global optima of the curves. The wideband behavior of the proposed device is clearly demonstrated since its performance does not vary substantially with the deviation of the arbitrary operational frequency ω from ω_0. Furthermore, for the circle-circle and circle-triangle geometries, the radiation is stable when the position of the source changes (Fig. 7(b)). The decay of enhancement with increasing L for the triangle-triangle design takes place because the source is moved away from the optimal position when the cut corresponds to the radiating cone position and orientation. In other words, the beneficial effect of the structure is not substantially dependent on the exact position of the source.

In Fig. 8, we show typical spatial distributions of the electric field for the three design solutions. Dramatic enhancement of radiation is obvious, especially for the triangle-triangle configuration (Fig. 8(a)). We can observe that strong concentration and enhancement takes place not only behind the antenna structure, but also in the reflected field. This finding means that the enhancement factor $\mathcal{EUR}$ would be larger if the overall radiation around the structure was taken into account (instead of confining the computation at the rear side of the HMM). The saturation of the figure may be attributed to the finite meshing of the simulation software. It is instructive to compare this phenomenon with reflection from corner reflectors (formed by electric or magnetic walls as limiting cases) and see how our device outperforms conventional concepts. Since the distance from the source to the reflector is very small ($0.1\lambda_0$), the radiated field in the left half-space can be found using the image principle as the sum of two very closely positioned dipole sources. The amplitude of the total dipole moment can vary from zero to the double value of that of the source dipole. Thus, there could not be neither directed beam nor any significant radiation enhancement for any reflection coefficient of the

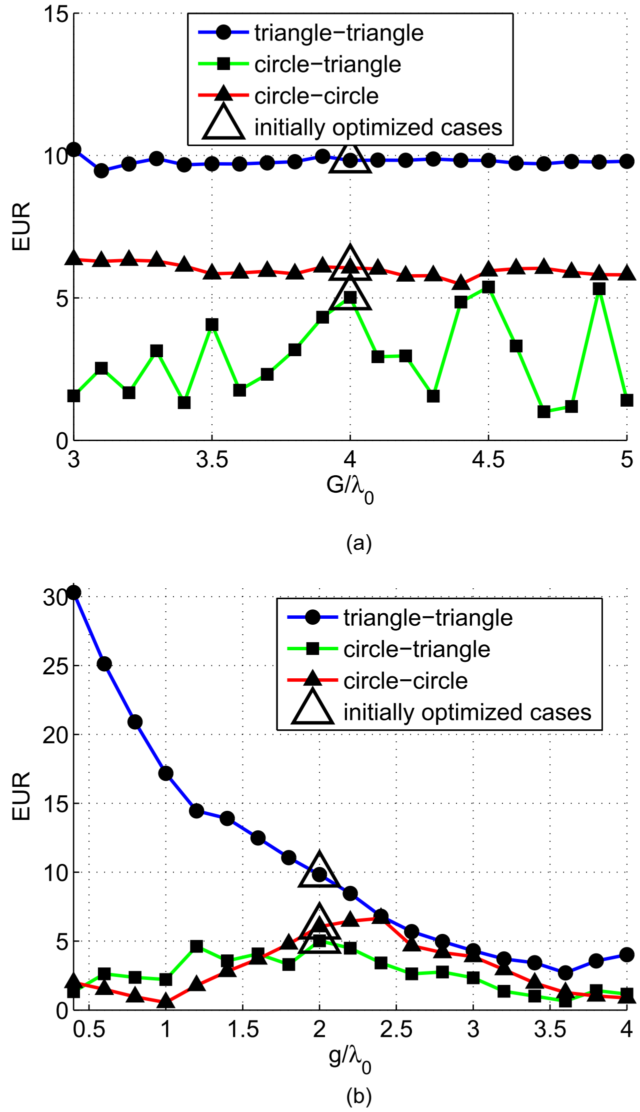

FIG. 7. The stability of the optimized structures with respect to frequency and source location. Triangle-triangle design (Fig. 5(a)) blue curves with circular dots, circle-triangle design (Fig. 5(b)) green curves with square dots, circle-circle design (Fig. 5(c)) red curves with triangular dots. (a) $\mathcal{EUR}$ as function of the normalized frequency ω/ω_0 (ω_0 is the frequency for which the optimization was done). (b) $\mathcal{EUR}$ as function of L/λ_0. Design parameters ensure the same $\mathcal{EUR}$ as is expected for macroscopic samples beside the circle-triangle sample. The selected optimized cases are denoted by black triangles.

corner reflector. On the contrary, the field distribution in Fig. 8(a) clearly shows that the whole surface of the triangular cut is strongly excited and creates radiated fields in free space. This results in a strong and directed beam.

In Sec. III B, we consider grooves shaped as spherical segments which represent a 3D generalization of the circle-circle structure.

B. 3D geometry

Since the effect for the transmitted field through the circle-circle structure depicted in Fig. 4(a) is similar to the effect for the reflected field in the case shown in Fig. 4(b), we restrict our study to the case of a perfect mirror behind the HMM sample. We investigate a sample of HMM whose

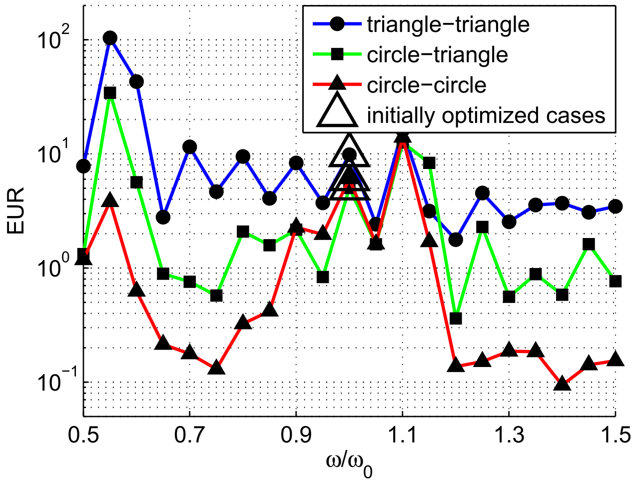

(a)

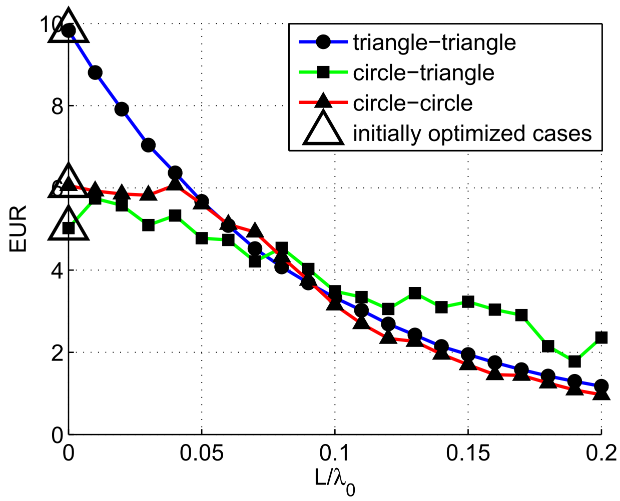

(b)

FIG. 8. Spatial distributions of the electric field magnitude for: (a) the triangle-triangle structure, (b) the circle-triangle structure, and (c) the circle-circle structure.

geometry is presented in Fig. 9. The simulation software for the 3D problem is the ANSYS HFSS package[28] and these simulations are much more time consuming than the 2D simulations described above. Therefore, we essentially used the results of our previous studies in order to minimize the amount of our 3D simulations.

Besides of choosing *a priori* the spherical segment shape for the groove, we have also preselected the vertical orientation of the negative optical axis and the vertical orientation of the emitting point dipole. Since the z axis is normal to the mirror plane, the negative component $\varepsilon_{||}$ of the permittivity tensor corresponds to the z-axis, whereas $\varepsilon_{\perp}$ corresponds to the xy plane. The structure is excited by a z-polarized Hertzian dipole located on the metamaterial boundary. This choice fits an explicit implementation of the HMM sample which appears to be feasible using the existing technologies. In particular, such HMM can be fabricated as a set of vertical silver or gold nanowires grown in vertically aligned pores or holes. Nanoholes of diameter 50–100 nm can be prepared in the area of several square millimeters using electrochemical etching.[29] Nanowires of diameter 20–50 nm can be fabricated using track membranes influenced by an ion beam.[30] As far as the metal inside nanopores of a porous sample is concerned, it is introduced using electrochemical deposition. In this way, one prepares arrays of aligned nanowires in flat layers of optical glass, anodic aluminum oxide, polymer and semiconductors.[31–34] In our opinion, the curvature of the interface should not obstruct the application of these technologies, since its radius is assumed to be sufficiently large. First, one prepares the vertical nanopores in a flat layer of a host medium, then one mechanically makes a macroscopic groove in it and finally one may electrochemically deposit metal into the nanopores.

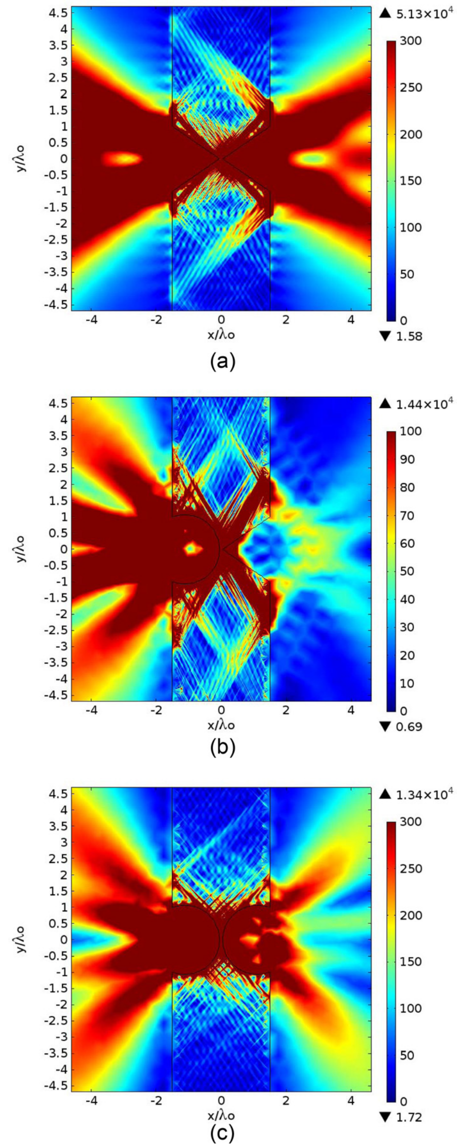

FIG. 9. The 3D structure under numerical investigation (side view). The negative axis of the HMM sample with the length $G \gg \lambda_0$ is orthogonal to the structure. The groove is a spherical segment of depth $g/2$ which transits into a hemisphere if $s = 0$.

The full-wave simulation of a macroscopic groove is again not possible; therefore, we have thoroughly studied the trends for $\mathcal{EUR}$ increasing the curvature radius of the groove $(s + g/2)$ up to $9\lambda_0$. Also, we increased the overall size G of the sample up to $8\lambda_0$. In three dimensions, we define the enhancement of useful radiation as

$$\mathcal{EUR} = \lim_{R\to+\infty} \frac{\int_0^{\pi/2}\int_0^{2\pi} |\mathbf{E}(R,\theta,\phi)|^2 d\phi d\theta}{\int_0^{\pi/2}\int_0^{2\pi} |\tilde{\mathbf{E}}(R,\theta,\phi)|^2 d\phi d\theta}, \tag{6}$$

where $\mathbf{E}$ and $\tilde{\mathbf{E}}$ are the electric fields of the dipole source in presence and absence of the HMM sample, respectively. Apparently, $R = \sqrt{x^2+y^2+z^2}$, $\phi = \arctan(x,y)$ and $\theta = \arccos(z/\sqrt{x^2+y^2+z^2})$ are the spherical coordinates of the observation point (x, y, z). If the PEC (Perfect Electric Conductor)-backed hyperbolic material is not present, the far-zone electric field of a Hertzian dipole in the absence of the PEC patch (dimensions $G \times G$) has a single θ component given by the analytical expression:

$$\tilde{\mathbf{E}}(R,\theta,\phi) = \hat{\theta}\, A \frac{e^{-jk_0R}}{k_0R} \sin\theta. \tag{7}$$

Since we consider a more realistic case than in the previous parts, let us discuss the electromagnetic properties of HMM of gold nanowires located in a lossless dielectric host of permittivity ε_h. Based on the well-known mixing formulas, the transverse and the axial components of the permittivity tensor are given, respectively, by[35]

$$\varepsilon_\perp = \varepsilon_h \frac{(\varepsilon_m + \varepsilon_h) + f_v(\varepsilon_m - \varepsilon_h)}{(\varepsilon_m + \varepsilon_h) - f_v(\varepsilon_m - \varepsilon_h)}, \tag{8}$$

$$\varepsilon_\parallel = f_v\varepsilon_m + (1 - f_v)\varepsilon_h, \tag{9}$$

where ε_m is the complex permittivity of gold, $f_v = \pi r_0^2/a^2$ is the filling factor of metal in HMM (r_0 is the wire radius, a is the array period). To estimate the permittivity of gold, we use the well-known Drude model

$$\varepsilon_m = \varepsilon_\infty - \frac{\omega_p^2\varepsilon_0}{\omega(\omega - j\gamma)} \tag{10}$$

with the following model parameters:[36] $\varepsilon_\infty \approx 9.5\varepsilon_0$, $\omega_p = 1367$ Trad/s, and $\gamma = 105$ Trad/s. The parameters to be optimized are the minimal thickness $d/2$, parameter s determining the groove shape, and the filling fraction of nanowires f_v. The wavelength for the optimization is the same as above: $\lambda_0 = 1\ \mu$m ($\omega_0 = 600\pi$ Trad/s). For $r_0/a = 0.25$ and host medium $\varepsilon_h \approx 2\varepsilon_0$, we obtain using (8)–(10)

$$\varepsilon_\perp \approx (3.1 - j0.009)\varepsilon_0, \tag{11}$$

$$\varepsilon_\parallel \approx -(6.8 + j0.6)\varepsilon_0. \tag{12}$$

One could point out that due to the finite periodicity of the underlying structure will impose a cut-off limit for the wavenumber above which the homogeneous description is no more valid. However, in the consider cases the losses in the wire-medium HMM have much more impact than the internal granularity. In fact, taking into account granularity will change nothing in the background of so high losses since they already cancel the contribution of spatial harmonics with spatial frequencies higher than the inverse period of the wire medium.

The optimization of the filling fraction within the interval $0.1 < f_v < 0.4$ keeping the host medium permittivity within the interval $1.7\varepsilon_0 < \varepsilon_h < 10\varepsilon_0$ keeps the same order for real and imaginary parts of these components of the permittivity tensor as in (11) and (12), respectively. The interval $1.7\varepsilon_0 < \varepsilon_h < 10\varepsilon_0$ corresponds to available solid media with negligible losses in the vicinity of λ_0, namely within $0.7\,\mu\text{m} < \lambda_0 < 1.3\,\mu\text{m}$. The condition $f_v < 0.4$ corresponds to applicability of the effective-medium model, and $f_v > 0.1$ corresponds to the regime of HMM $\Re[\varepsilon_\parallel] < 0$, $\Re[\varepsilon_\perp] > 0$ for the wire medium in such host within the considered interval of wavelengths. The relative freedom in ε_h and f_v allows us to optimize $\mathcal{EUR}$ in terms of $|\Re[\varepsilon_\parallel]|/\Re[\varepsilon_\perp]$ as it was done above. Indeed, at frequency ω_0, the formulas (8) and (9) allow realistic values for f_v and ε_h for any ratio $|\Re[\varepsilon_\parallel]|/\Re[\varepsilon_\perp]$ laying within the interval $1 < |\Re[\varepsilon_\parallel]|/\Re[\varepsilon_\perp] < 5$ which is sufficient for optimization.

In this 3D case, we followed an inverse optimization approach compared to the 2D case. First, we fixed $\varepsilon_\perp = (3.1 - j0.009)\varepsilon_0$ and $\varepsilon_\parallel = (-6.8 - j0.6)\varepsilon_0$ and for preselected geometric parameters $G = 8\lambda_0$, $s = L = 0$, $d = 0.5\lambda_0$ studied the trend of $\mathcal{EUR}$ versus g/λ_0 (Fig. 10(a)), based on the assumption that the optimal permittivities would be not far from the initial choice. It should be pointed out that there is no reason for Fig. 10(a) to be similar to the curve of the two circular notches of Fig. 11(b) since the latter one is referred to a two-dimensional configuration with no PEC backing and with different dimensions and materials. It is clear that resonances hold only for $g < 1.6\lambda_0$, oscillation versus g are small and their averaged value corresponds to $g = 2\lambda_0$. For this case, we show the color map of the field intensity in Fig. 10(b). On this map, one can clearly see two rays corresponding to the radiation cones below the spherical notch which issymmetric with respect to the z axis. These rays, reflected by the mirror, experience partial internal reflection at the interface of HMM, which happens simultaneously with a strong transmission of waves from the metamaterial to free space. Thus, the groove diameter $g = 2\lambda_0$ is not a relevant parameter, and our expectations based on the geometrical optics are fully justified. In a sense, we have

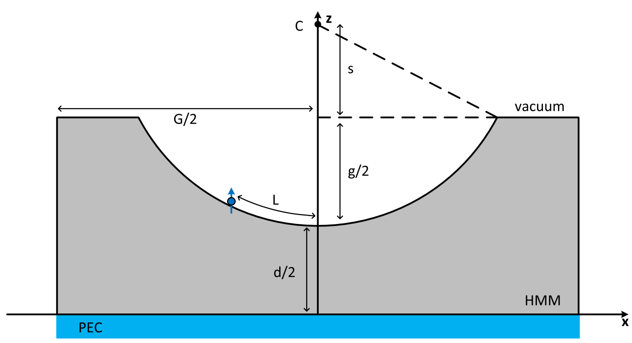

FIG. 10. (a) The trend for $\mathcal{EUR}$ when the groove diameter g increases. Plot parameters: $\Re[\varepsilon_\perp] = 3.1\varepsilon_0$, $\Re[\varepsilon_\parallel] = -6.8\varepsilon_0$, $d = 0.5\lambda_0$, $G = 8\lambda_0$, $s = L = 0$. (b) The field distribution over the vertical cross section of the HMM sample shows the absence of resonance and confirms the adequacy of geometric optics for $g = 2\lambda_0$.

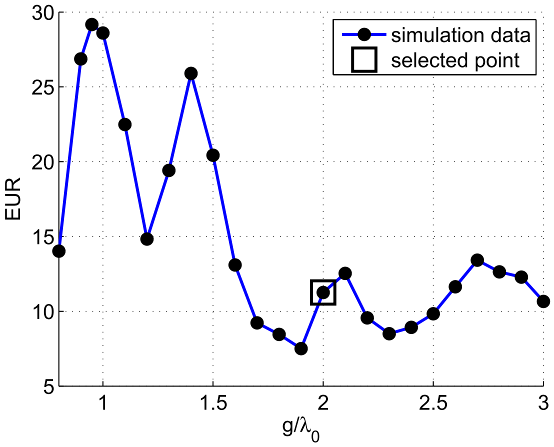

(a)

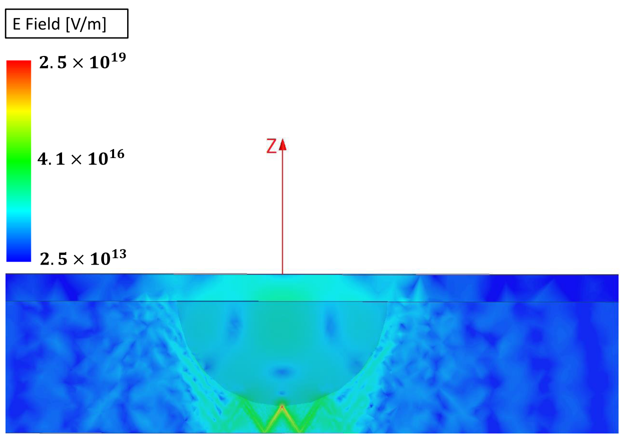

(b)

FIG. 11. Search of the macroscopic trend for $\mathcal{EUR}$ versus: (a) the overall size G and (b) the cut size g. The optimal designs from Fig. 6, denoted by black triangles are tested. Triangle-triangle design (Fig. 5(a)) blue curves with circular dots, circle-triangle design (Fig. 5(b)) green curves with square dots, circle-circle design (Fig. 5(c)) red curves with triangular dots. The selected optimized cases are denoted by black triangles.

"optimized" the distance g in order not to coincide with a local resonance. The same $\mathcal{EUR}$ is expected for macroscopic values $g \gg \lambda_0$ if the groove is hemispheric.

The permittivity ratio $|\Re[\varepsilon_{||}]|/\Re[\varepsilon_{\perp}]$ has been also optimized. The dependence of $\mathcal{EUR}$ on this ratio is shown in Fig. 12(a), where the optimum corresponds to $\Re[\varepsilon_{||}] = -10.5$, $\Re[\varepsilon_{\perp}] = 3.1$; that implies the metal fraction $f_v = 0.27$ and the host medium permittivity $\varepsilon_h = 1.7$. For these parameters, we optimized the minimal thickness of HMM $d/2$. We have checked three values of the minimal thickness $d/2 = 0.05\lambda_0$, $0.25\lambda_0$ and $0.5\lambda_0$; the best choice is $g/2 = 0.25\lambda_0$. With the aforementioned selection of $d/2$ and the $\Re[\epsilon_{||}]$, $\Re[\epsilon_{\perp}]$, we optimized the shape of the spherical segment, varying the parameter s (Fig. 12(a)); the best result corresponds to the hemisphere when $s = 0$. However, for $s > 2\lambda_0$ another possibility to achieve a rather high value of $\mathcal{EUR}$ (namely $\mathcal{EUR} = 7$) is emerging. To exploit it, we have to fix the groove depth $g = 2\lambda_0$ and prepare its shape as a thin spherical segment with an arbitrary macroscopic radius. Such sample is easier to fabricate than the structure with a hemispheric notch, but the enhancing effect is less substantial.

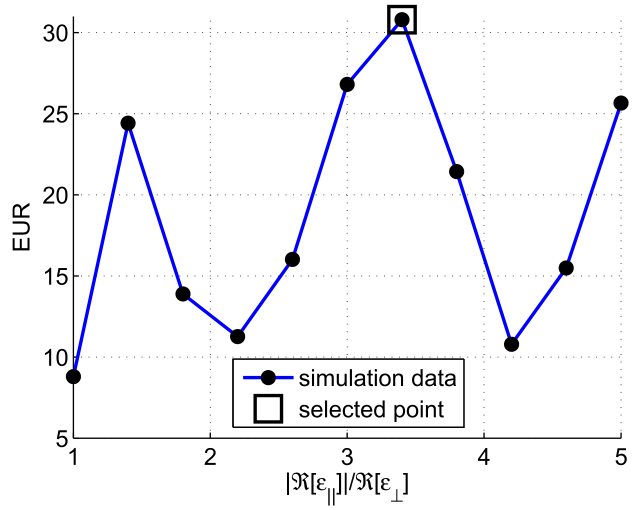

(a)

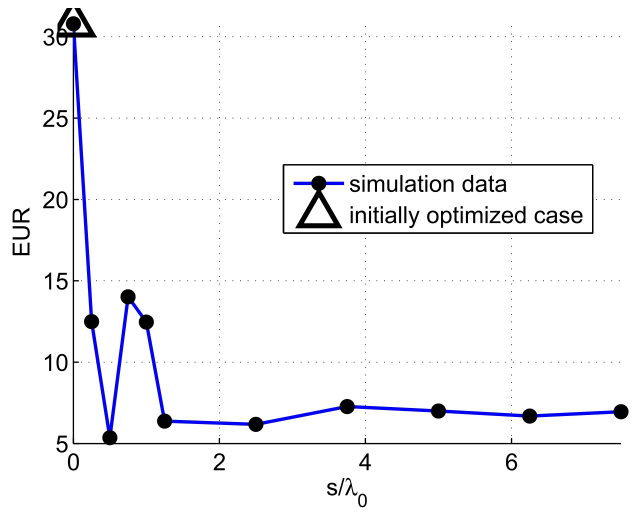

(b)

FIG. 12. The optimization graphs for the 3D structure. (a) $\mathcal{EUR}$ versus $|\Re[\varepsilon_{||}]|/\Re[\varepsilon_{\perp}]$. Fixed plot parameters: $\Re[\varepsilon_{\perp}] = 3.1\varepsilon_0$, $d = 0.5\lambda_0$, $G = 8\lambda_0$, $L = 0$, $g = 2\lambda_0$, $\omega = \omega_0 = 600\pi$ Trad/s. (b) $\mathcal{EUR}$ versus the parameter s/λ_0 for $\Re[\varepsilon_{\perp}] = 3.1\varepsilon_0$, $\Re[\varepsilon_{||}] = -10.5\varepsilon_0$, $d = 0.5\lambda_0$, $G = 8\lambda_0$, $g = 2\lambda_0$.

We have checked that for $G = 6\lambda_0$ the results did not change compared to those obtained for $G = 8\lambda_0$; thus, we really have found the macroscopic trend. The stability of the effect with respect to the frequency deviation is illustrated by Fig. 13(a). One readily observes that at least one order of magnitude enhancement corresponds to the interval $0.7\,\omega_0 < \lambda_0 < 1.3\,\omega_0$. For the optimal structure ($\mathcal{EUR} = 30$) we have checked that $\mathcal{EUR}$ keeps larger than 15 for $L \geq g/25$, i.e., 80 nm. More importantly, within the interval $L = \pm g/57$ (that in the present case implies $L = 35$ nm), $\mathcal{EUR}$ keeps stable and practically equals 30. In Fig. 13(b), we show the radiation pattern for the case $L = 35$ nm. The deformation of this pattern due to an asymmetric location of the source can be better estimated in comparison with the pattern for $L = 0$ of Fig. 13(c). The absence of zenithal radiation results from the vertical orientation of the dipole. The radiation to the lower half-space is small due to the presence of the mirror, but it is nonzero due to a finite value of G. We can see that the presence of the HMM sample makes the

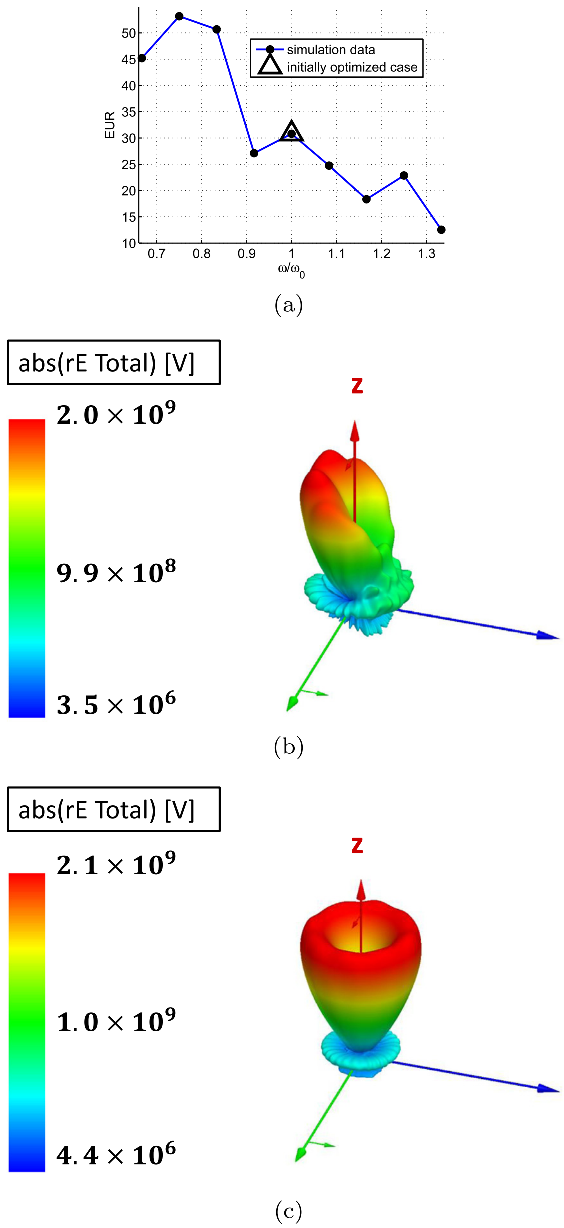

FIG. 13. (a) $\mathcal{EUR}$ of the optimized structure versus the frequency deviation. (b) The radiation pattern of a dipole located at the point $L = 35$ nm in comparison to that of the same dipole located at the point $L = 0$ (c).

far-field radiation of the dipole quite directional. This directionality is not destroyed by reasonably small displacements of the source, which is another evidence that the radiation enhancement is only weakly sensitive to the source positioning.

In summary, we have confirmed that a hemispherical macroscopic groove prepared in a layer of HMM allows very strong (1-2 orders of magnitude) enhancement of useful emission for dipole sources located close to the bottom of the groove. The emission enhancement keeps high in a broad frequency range and for noticeable (though much smaller than the groove diameter) displacements of the source from the groove center. This enhanced power in radiated into a tight beam forming a cone in free space for sources distributed symmetrically in the vicinity on the bottom point. A significant enhancement can be achieved also with a groove shaped as a thin spherical segment with an optically large diameter. It is important that the effect is achievable in a practically feasible variant of HMM, which can be performed as an array of gold nanowires in a porous matrix.

IV. CONCLUSIONS

In this paper, we have shown that macroscopic samples of hyperbolic metamaterials can be shaped so that they constitute effective antennas, transforming evanescent fields (produced by nanoemitters) into traveling waves in free space. These antennas effectively enhance radiation of small sources and, in addition, they are capable of creating directive beams radiating into vacuum. Here we utilize the phenomenon of conical radiating beams which are excited by small sources inside a hyperbolic medium samples or close to interfaces with such media. Understanding the orientation of the cones and using the knowledge on the isofrequency contours, we have found the appropriate shapes of the hyperbolic material sample as well as the orientation of the optical axis, which ensure that most of the power propagating in/across the cones is eventually radiated into free space. In contrast to earlier works on enhancement of point-source radiation using hyperbolic media, where the enhanced radiated power could not leave the volume of the hyperbolic media sample, the structures introduced here function as broadband antennas creating directive beams in free space. Furthermore, the enhancement of radiated power weakly depends on the position of nanosources, which is important for detection of emission from solutions or otherwise arbitrarily positioned objects. The shape and direction of the radiated beam, on the other hand, depends on the source position, which can be used for nano-precision position detection of a number of moving particles in real time.

[1]A. Kinkhabwala, Z. Yu, S. Fan, Y. Avlasevich, K. Mullen, and W. E. Moerner, Nature Photon. **3**, 654 (2009).
[2]R. Filter, K. Slowik, J. Straubel, F. Lederer, and C. Rockstuhl, Opt. Lett. **39**, 1246 (2014).
[3]C. Sauvan, J. P. Hugonin, I. S. Maksymov, and P. Lalanne, Phys. Rev. Lett. **110**, 237401 (2013).
[4]S. A. Schelkunoff and H. T. Friis, *Antennas Theory and Practice* (John Wiley & Sons, New York, 1952).
[5]A. Poddubny, I. Iorsh, P. Belov, and Y. Kivshar, Nature Photon. **7**, 948 (2013).
[6]D. R. Smith and D. Schurig, Phys. Rev. Lett. **90**, 077405 (2003).
[7]F. V. Bunkin, J. Exp. Theor. Phys. **32**, 338 (1957).
[8]A. G. Sitenko and K. N. Stepanov, J. Exp. Theor. Phys. **31**, 642 (1956).
[9]B. P. Kononov, A. A. Rukhadze, and G. V. Solodukhov, Sov. Phys.: Tech. Phys. **6**, 405 (1961).
[10]R. K. Fisher and R. W. Gould, Phys. Rev. Lett. **22**, 1093 (1969).
[11]L. Felsen and N. Marcuvitz, *Radiation and Scattering of Waves* (Prentice Hall, New York, 1972).
[12]L. Felsen, *Radiation and Scattering of Waves* (IEEE Press Series on Electromagnetic Wave Theory, New York, 1972).
[13]A. N. Poddubny, P. A. Belov, and Y. S. Kivshar, Phys. Rev. A **84**, 023807 (2011).
[14]A. N. Poddubny, P. A. Belov, P. Ginzburg, A. V. Zayats, and Y. S. Kivshar, Phys. Rev. B **86**, 035148 (2012).
[15]T. U. Tumkur, L. Gu, J. K. Kitur, E. E. Narimanov, and M. A. Noginov, Appl. Phys. Lett. **100**, 161103 (2012).
[16]A. N. Poddubny, P. A. Belov, and Y. S. Kivshar, Phys. Rev. B **87**, 035136 (2013).
[17]J. Kim, V. P. Drachev, Z. Jacob, G. V. Naik, A. Boltasseva, E. E. Narimanov, and V. M. Shalaev, Opt. Exp. **20**, 8100 (2012).

[18]D. Lu, J. J. Kan, E. E. Fullerton, and Z. Liu, Nature Nanotechnol. **9**, 48 (2014).
[19]S. Mittler-Neher, J. Spinke, M. Liley, G. Nelles, M. Weisser, R. Back, G. Wenz, and W. Knoll, Biosensors Bioelectron. **10**, 903 (1995).
[20]E. E. Narimanov, H. Li, Y. A. Barnakov, T. U. Tumkur, and M. A. Noginov, Opt. Exp. **21**, 14956 (2013).
[21]C. A. Valagiannopoulos and C. R. Simovski, "Conversion of evanescent waves into propagating modes by passing through a metamaterial prism: an iterative approximation method," in *Proceedings of the 5th European Conference on Antennas and Propagation (EUCAP), Rome* (2011), p. 103.
[22]C. A. Valagiannopoulos and C. R. Simovski, Radio Sci. **47**, RS6004, doi:10.1029/2012RS005052 (2012).
[23]A. Salandrino and N. Engheta, Phys. Rev. B **74**, 075103 (2006).
[24]D. Lu and Z. Liu, Nature Commun. **3**, 1205 (2012).
[25]S. M. Hashemi and I. S. Nefedov, Phys. Rev. B **86**, 195411 (2012).
[26]I. S. Nefedov, C. A. Valagiannopoulos, S. M. Hashemi, and E. I. Nefedov, Sci. Rep. **3**, 2662 (2013).
[27]See www.comsol.com for COMSOL Multiphysics.
[28]www.ansys.com, website of Ansys HFSS.
[29]M. Sailor, *Porous Silicon in Practice: Preparation, Characterization and Applications* (Wiley-VCH: Hoboken, New Jersey, 2010).
[30]R. Spohr, *Ion Tracks and Microtechnology: Principles and Applications* (Vieweg, Braunschweig, 1990).
[31]A. G. Cullis, L. T. Canham, and P. D. J. Calcott, J. Appl. Phys. **82**, 909 (1997).
[32]P. A. Smith, C. D. Nordquist, T. N. Jackson, and T. S. Mayer, Appl. Phys. Lett. **77**, 1399 (2000).
[33]P. Evans, W. R. Hendren, R. Atkinson, G. A. Wurtz, W. Dickson, A. V. Zayats, and R. J. Pollard, Nanotechnology **17**, 5746 (2006).
[34]V. P. Ulin and S. G. Konnikov, Semiconductors **41**, 832 (2007).
[35]A. Sihvola, *Electromagnetic Mixing Formulae and Applications* (IEEE Electromagnetic Waves Series, New York, 1999).
[36]R. L. Olmon, B. Slovick, T. W. Johnson, D. Shelton, S.-H. Oh, G. D. Boreman, and M. B. Raschke, Phys. Rev. B **86**, 235147 (2012).